Journal of the European Ceramic Society xxx (xxxx) xxx–xxx

Contents lists available at ScienceDirect

Journal of the European Ceramic Society

journal homepage: www.elsevier.com/locate/jeurceramsoc

Original Article

A new Li-based ceramic of $Li_4MgSn_2O_7$: Synthesis, phase evolution and microwave dielectric properties

Ruzhong Zuo*, He Qi, Fang Qin, Qianlong Dai

Institute of Electro Ceramics & Devices, School of Materials Science and Engineering, Hefei University of Technology, Hefei, 230009, PR China

ARTICLE INFO

Keywords:
Microwave dielectric property
LTCC
Single phase
Li-based compounds

ABSTRACT

A pure-phase $Li_4MgSn_2O_7$ (L_4MS) was successfully synthesized through optimizing the calcination condition. Microwave dielectric properties of the L_4MS ceramic with the phase evolution were investigated together with its low-temperature sintering. The sample maintains a single L_4MS phase as sintered below 1200 °C, such that τ_f remains a constant value of ~12.4 ppm/°C. Accompanied by the appearance of impurity phases $(Li_2SnO_3)_{ss}$ and especially $(MgO)_{ss}$ at higher sintering temperatures, excellent microwave dielectric properties of ε_r = 13.1–13.5, Q × f = 106,800–126,810 GHz and τ_f = 0–−4.2 ppm/°C are obtained in samples sintered at 1215–1260 °C for 4 h. Reduction of sintering temperature using LiF sintering aid also helps achieve pure-phase dense L_4MS ceramic. The L_4MS + x wt.% LiF ceramic exhibits ε_r ~13.7, Qxf ~97,000 GHz (x ≤ 3) and τ_f ~8–13 ppm/°C sintered at 850 °C for potential LTCC applications, and ε_r ~13.9, Qxf ~146,000 GHz and τ_f ~1.5–6 ppm/°C (x ≥ 4) as sintered 1000 °C, exhibiting large potentials for microwave dielectric candidates.

1. Introduction

The Li-based rock-salt structured materials have gained considerable attention in recent years for their large potentials in microwave devices. Li_2TiO_3 gained relatively early attention as possible microwave dielectric candidate materials, followed by its counterparts such as Li_2SnO_3 and Li_2ZrO_3 [1–3]. Although these Li_2BO_3 ceramics are expected to have desirable electrical properties, yet poor microstructure and even microcracks have seriously impeded their potential applications in microwave devices owing to both the easy cleavage on (001) plane and the lithium evaporation at higher sintering temperatures [1–4]. Different ways have been attempted to solve the above issues such as Li-rich atmosphere protection [5,6], liquid-phase sintering [3,7,8] or forming solid solutions with other materials such as MgO, ZnO or NiO [4,9–13], generating significantly improved microwave dielectric properties. In addition, a couple of microwave dielectric materials in Li_2BO_3-AO (B: Sn, Ti, Zr; A: Mg, Zn, Ni) systems have been reported in recent years to exhibit excellent microwave dielectric properties [9,13,14], including Li_2BO_3 solid solutions ($(Li_2BO_3)_{ss}$, AO-structured solid solutions ($(AO)_{ss}$) and/or some compounds [6,7,13–21]. These solid solution ceramics either exhibit a positive temperature coefficient of resonant frequency (τ_f) at the Li_2BO_3-rich side or a negative τ_f at the AO-rich side except for their low-loss features. Among them, $Li_2Mg_3BO_6$ (B: Ti, Sn, Zr) ceramics belonging to the $(MgO)_{ss}$ possess excellent microwave dielectric properties of ε_r = 15.2, 8.8 and 12.6, Qxf = 152,000 GHz (at 8.3 GHz), 123,000 GHz (at 10.7 GHz) and 86,000 GHz (at 9.3 GHz), and τ_f = −39 ppm/°C, −32 ppm/°C and −36 ppm/°C, respectively, at their optimal sintering temperatures [14,16,22]. A higher Qxf value of ~230,000 ~330,000 GHz was reported in well-densified $Li_2Mg_3SnO_6$ ceramics by means of sintering aids [7].

As early as 1984, the phase diagram of the $Li_{2/3(1-x)}Sn_{1/3(1-x)}Mg_xO$ system was proposed by M. Castellanos and A. R. West [23], in which a β-$(Li_2SnO_3)_{ss}$ single-phase zone, a two-phase zone of β-$(Li_2SnO_3)_{ss}$, $Li_4MgSn_2O_7$ (L_4MS) compound, a wide $(MgO)_{ss}$ single-phase zone, and an additional two-phase zone of $(MgO)_{ss}$ and L_4MS. Recently, the phase structure was further investigated in this system within a wide composition range of x = 0–4/7 except for microwave dielectric properties of some special compositions as reported previously [13]. Of special note is that as new potential dielectric material, microwave dielectric properties of the L_4MS compound has never been reported, although it appears for the first time in the phase diagram of $LiSnO_3$-MgO, and also but only exists later as an impurity phase in some previous studies [7,13,23,24]. The possible reasons might be ascribed to difficulties in pure-phase synthesis and densification behaviors like other Li-based systems [20–26]. In this work, the synthesis processing and sintering of L_4MS ceramics were investigated by means of a conventional solid-state method. Relationship between the phase structure, microstructure and

* Corresponding author.
E-mail address: piezolab@hfut.edu.cn (R. Zuo).

https://doi.org/10.1016/j.jeurceramsoc.2018.08.019
Received 29 June 2018; Received in revised form 13 August 2018; Accepted 16 August 2018

microwave dielectric properties was discussed in detail, together with a low-temperature firing of L_4MS ceramics at a temperature of 850 °C.

2. Experimental procedures

The L_4MS ceramics were synthesized by a traditional solid-state reaction method. High-purity powders of MgO, SnO_2 and Li_2CO_3 were used as starting materials. Stoichiometric amounts of the powders were weighed and ball-milled for 10 h using zirconia balls and alcohol as the medium on a planetary milling machine. The resulting slurries were then rapidly dried and calcined at 850–1050 °C for 8–16 h in air. The calcined powders were re-milled for 10 h and then mixed together with 5 wt% PVA as a binder. The granulated powders were subsequently pressed into cylinders with dimensions of 10 mm in diameter and 7–8 mm in height. The specimens were first heated at 550 °C in air for 4 h to remove the organic binder, and then sintered at 1120 °C–1275 °C for 4 h. Moreover, the x wt.% LiF sintering aid was added into the as-synthesized pure-phase L_4MS powder and then experienced a sufficient mixing process in alcohol. The L_4MS + x wt.% LiF samples were sintered in air at 800–1075 °C for 4 h. The heating rate was 5 °C/min, and the cooling rate was 10 °C/min. The compacts were muffled with powders of the same composition in an upturned alumina crucible to suppress the lithium evaporation.

The crystal structure of the fired ceramics was identified via an X-ray diffractometer (XRD, D/Max2500 V, Rigaku, Japan) using Cu $K\alpha$ radiation. Rietveld refinements on full profiles of XRD patterns were performed by using the program GSAS to identify the structural parameters of each phase. The bulk densities of the sintered ceramics were measured by the Archimedes method. The microstructure of the pellets was observed using a field-emission scanning electron microscope (FE-SEM; SU8020, JEOL, Tokyo, Japan) equipped with an energy dispersive spectrometer (EDS). For the observation of grain morphology, the samples were polished and then thermally etched at a temperature 150 °C lower than the respective sintering temperature for 30 min. Microwave dielectric properties of the ceramic cylinders were measured using a network analyzer (N5230C, Agilent, Palo Alto, CA) and a temperature chamber (GDW-100, Saiweisi, Changzhou, China). The τ_f values of the samples were measured in the temperature range from 20 °C to 80 °C and calculated by the following equation:

$$\tau_f = \frac{f_2 - f_1}{f_1(T_2 - T_1)} \quad (1)$$

where f_1 and f_2 represent the resonant frequencies at T_1 and T_2, respectively.

3. Results and discussion

Fig. 1 shows the XRD patterns of the stoichiometric L_4MS powders calcined under different conditions. Compared with the standard patterns of JCPDS # 31–0761 and JCPDS # 37–1164, it can be seen that Li_2SnO_3 is a dominant phase apart from a slight amount of L_4MS phase as it was calcined at 850 °C for 8 h. With increasing the calcination temperature, L_4MS obviously increases in its phase content, and becomes a main phase in addition to some residual Li_2SnO_3 as the calcination condition is 1050 °C for 8 h, indicating L_4MS has a higher phase formation temperature than Li_2SnO_3. The above results also demonstrate that Li_2O preferentially reacts with SnO_2 at a lower temperature. The reaction kinetic of the resulting Li_2SnO_3 with MgO is so sluggish that both higher calcination temperature and long calcination time are required. A slight amount of residual Li_2SnO_3 phase can be completely eliminated through the calcination at 1000 °C for 16 h, as shown in Fig. 1. Therefore, appropriate calcination temperature and time are two necessary conditions for the synthesis of pure L_4MS phase.

Fig. 2 illustrates normalized XRD patterns of L_4MS ceramics sintered at 1180 °C–1275 °C for 4 h using the pure-phase L_4MS powder. When

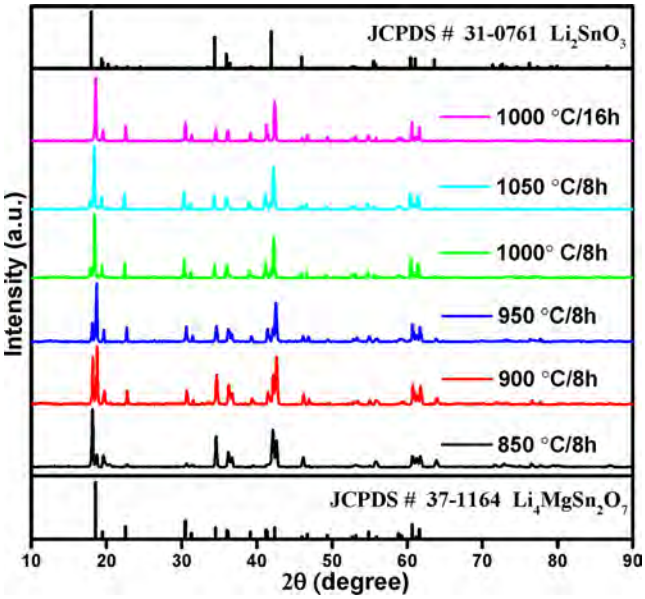

Fig. 1. XRD patterns of L_4MS specimens calcined under various conditions as indicated.

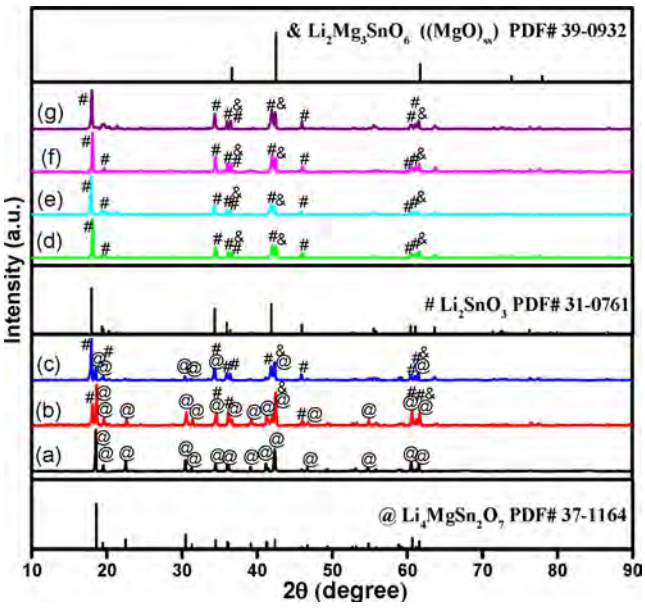

Fig. 2. XRD patterns of L_4MS ceramics sintered at various temperatures for 4 h: (a) 1180 °C, (b) 1200 °C, (c) 1215 °C, (d) 1230 °C, (e) 1245 °C, (f) 1260 °C and (g) 1275 °C.

sintering temperature is lower than 1200 °C, all diffraction peaks can be well indexed according to the L_4MS phase (JCPDS No. 37–1164) and no any other phase can be observed (Fig. 2(a)). An obvious secondary phase of $(Li_2SnO_3)_{ss}$ (JCPDS No. 31–0761) starts to appear as sintering temperature is higher than 1200 °C (Fig. 2(b–g)) and becomes more with further increasing sintering temperature. At the same time, another impurity phase of $(MgO)_{ss}$ (JCPDS No. 39–0932) can be also observed. As sintering temperature is higher than 1230 °C, the L_4MS phase nearly disappears and residual phases are $(MgO)_{ss}$ and $(Li_2SnO_3)_{ss}$ with varying phase content ratio with changing temperature. The phase content and the structure parameter of each phase can be obtained by means of Rietveld refinement of XRD patterns in Fig. 2. Only using samples in Fig. 2(d–g) owing to the lack of information about the unit cell and crystal structure of L_4MS phase, the Rietveld refinement patterns (only for the sample sintered at 1260 °C as an

Table 1
Refined structural parameters and reliability factors by using the Rietveld method for representative L_4MS samples sintered at different sintering temperatures (T_s) for 4 h.

T_s (°C)	S.G.	Lattice parameters	Cell volume, V (Å^3)	Phase content (%)	R_{wp} (%)	R_p (%)	χ^2
1230	C2/c	a = 5.2817(4) Å, b = 9.1840(7) Å, c = 10.0094(9) Å, α = 90°, β = 100.181(7)°, γ = 90°	477.895(42)	55	11.58	9.58	3.62
	Fm-3 m	a = b = c = 4.2555(2) Å, α = β = γ = 90°	77.066(8)	45			
1245	C2/c	a = 5.2838(5) Å, b = 9.1804(7) Å, c = 10.0114(9) Å, α = 90°, β = 100.304(8)°, γ = 90°	477.808(44)	48	11.28	9.22	3.35
	Fm-3 m	a = b = c = 4.2569(2) Å, α = β = γ = 90°	77.141(9)	52			
1260	C2/c	a = 5.2846(4) Å, b = 9.1764(7) Å, c = 10.0121(9) Å, α = 90°, β = 100.288(7)°, γ = 90°	477.729(41)	42	11.04	8.88	4.06
	Fm-3 m	a = b = c = 4.2574(2) Å, α = β = γ = 90°	77.171(9)	58			
1275	C2/c	a = 5.2852(4) Å, b = 9.1753(6) Å, c = 10.0125(7) Å, α = 90°, β = 100.351(6)°, γ = 90°	477.644(34)	33	10.48	9.00	4.68
	Fm-3 m	a = b = c = 4.2587(2) Å, α = β = γ = 90°	77.238(8)	67			

example) and corresponding structural parameters are shown in Fig. S1 and Table 1, in which R_{wp} is the reliability factor of weighted patterns, R_p is the reliability factor of patterns, and χ^2 is the goodness-of-fit indicator. The refinement results were found to best fit to a combination of C2/c ($(Li_2SnO_3)_{ss}$) and Fm-3 m ($(MgO)_{ss}$) space groups (S.G.) with acceptable reliability. The phase content of $(MgO)_{ss}$ is found to slightly increase with increasing sintering temperature. Compared with $(MgO)_{ss}$, the lattice parameters of $(Li_2SnO_3)_{ss}$ hardly change. These observations are basically due to the decomposition of L_4MS, and generally keep agreement with results in the Li_2SnO_3-MgO phase diagram [23]. The variation of the phase composition with varying sintering temperature might exert some influences on the final microwave dielectric properties.

The variation of bulk density and microwave dielectric properties of L_4MS ceramics as a function of sintering temperature is shown in Fig. 3(a). It is evident that the L_4MS sample exhibits a typical densification process with increasing sintering temperature. It reaches the maximum values approximately in the temperature range of 1220–1260 °C. Accompanied by the sample density variation, ε_r and Qxf values of the sintered ceramic show a monotonous increase with temperature (Fig. 3(b, c)). The similar trend with temperature indicates that the sample density should be a dominant factor influencing the permittivity and loss values although the phase composition may change as well with sintering temperature (Fig. 2). Also, these impurity phases observed in Fig. 2 might have similar dielectric properties (permittivity and Qxf values) to the main phase. In the first stage of sintering, a gradual increase in ε_r and Qxf is ascribed to the increase in sample density with increasing sintering temperature up to 1180 °C because the sample belongs to a single-phase L_4MS. Microwave dielectric properties of $\varepsilon_r = 12.4$, $Q \times f = 58{,}754$ GHz and $\tau_f = 12.1$ ppm/°C are obtained in the single-phase L_4MS ceramic as sintered at 1180 °C for 4 h, which might be underestimated to a certain degree owing to a low sample density. Because of the variation of phase composition with sintering temperature, the increase of ε_r and Qxf in the second and third stages can be ascribed to a combined effect of the phase coexistence and the increased sample density. Excellent microwave dielectric properties of $\varepsilon_r = 13.1$, $Q \times f = 106{,}800$ GHz, $\tau_f = 0.0$ ppm/°C, and $\varepsilon_r = 13.5$, $Q \times f = 126{,}810$ GHz, $\tau_f = -4.2$ ppm/°C are obtained in samples sintered at 1215 °C for 4 h and 1260 °C for 4 h, respectively. By comparison, τ_f exhibits an interesting change with changing sintering temperature, as shown in Fig. 3(d). In the single-phase zone, it remains a constant value of ~12.5 ppm/°C, indicating L_4MS has a positive τ_f value with an opposite sign to that of $(MgO)_{ss}$ including $Li_2Mg_3SnO_6$ [7,16,18]. Interestingly, τ_f value decreases monotonically from 12.1 to −5.9 ppm/°C when sintering temperature is above 1200 °C owing to the appearance of the $(MgO)_{ss}$ phase with a negative τ_f (for example, MgO: $\tau_f \sim -56$ ppm/°C [27]; $Li_2Mg_3SnO_6$: $\tau_f \sim -40$ ppm/°C [7]). The fact that $(MgO)_{ss}$ and $(Li_2SnO_3)_{ss}$ have good microwave dielectric properties [7,13,17,28] is also responsible for excellent electrical properties of L_4MS ceramics with impurity phases at higher sintering temperatures. It is obvious that the variation of τ_f values in the second and third stages might mainly depend on the change of phase composition. On the one hand, the $(Li_2SnO_3)_{ss}$ usually has a relatively small τ_f value and even becomes negative, compared to the Li_2SnO_3 compound [9]. On the other hand, compared with the $(Li_2SnO_3)_{ss}$ phase, the increasing amount of the impurity phase $(MgO)_{ss}$ with temperature (see Fig. 2 and Table 1) also helps tailor τ_f into negative values. A near-zero τ_f value can be thus obtained for samples sintered approximately at 1230 °C.

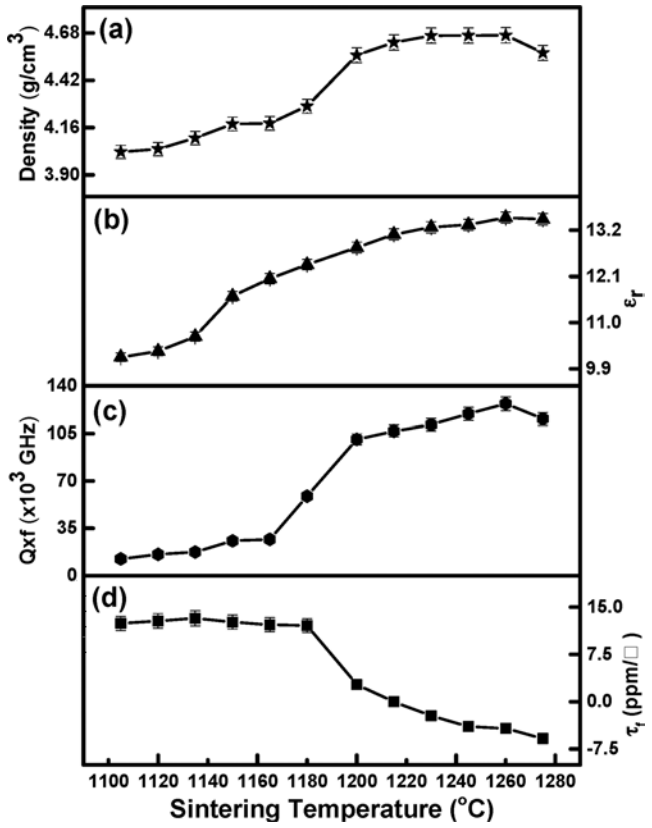

Fig. 3. Variation of (a) the sample density, (b) ε_r, (c) Qxf and (d) τ_f for L_4MS ceramics as a function of sintering temperature.

Fig. 4 demonstrates SEM images of L_4MS specimens sintered at different temperatures for 4 h. It can be seen that the ceramic specimen sintered at 1180 °C for 4 h exhibits typical uniform polygonal grains (Fig. 4(a)), corresponding to a single-phase L_4MS, as further confirmed by the EDS result (Fig. S2 and Table 2), in which the atom ratio of Sn to Mg is close to 2 (Grain A). A typical bimodal grain distribution can be observed in ceramic samples sintered at 1215 and 1260 °C, as shown in Fig. 4(b) and (c), respectively. In addition to a few polygonal grains, most of grains become short rod-like (Grain B and E) with a Sn:Mg raito of ~10 and ~4, respectively, typical of a Sn-rich $(Li_2SnO_3)_{ss}$. The former (polygonal grains) should belong to the L_4MS phase or $(MgO)_{ss}$ [7,13,23], but the latter proves to come from the impurity phase

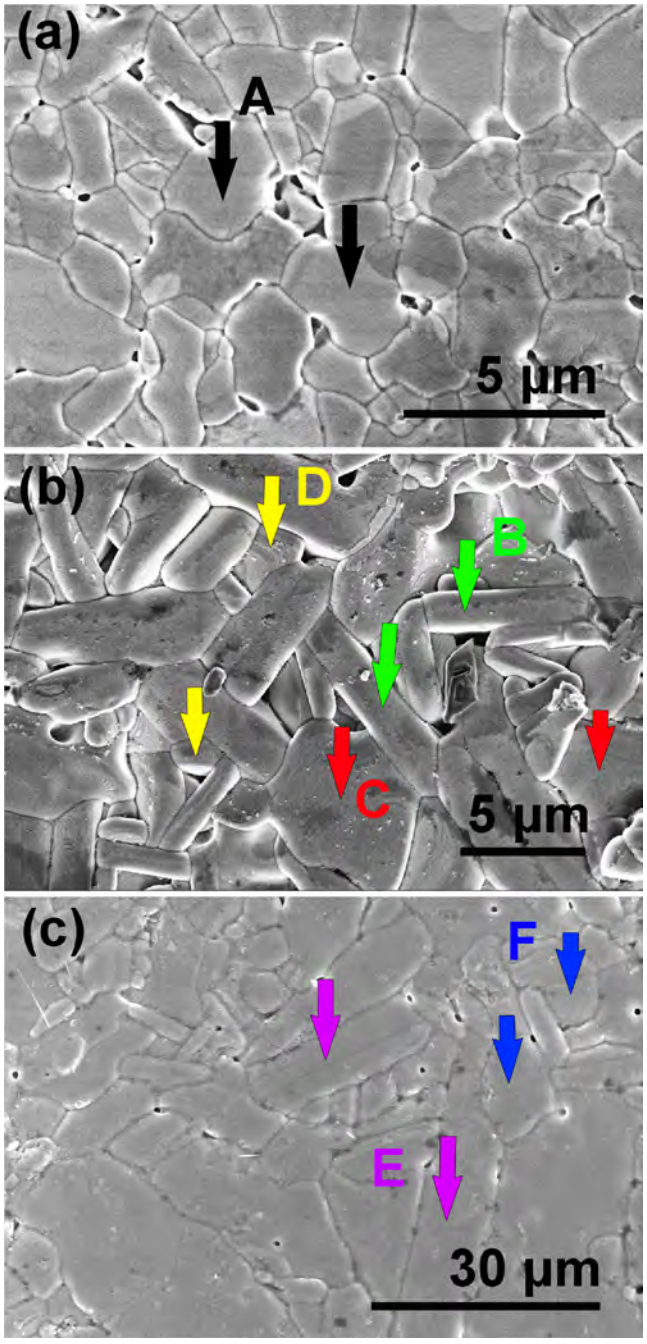

Fig. 4. SEM graphs of L_4MS ceramics sintered at various temperatures for 4 h: (a) 1180 °C, (b) 1215 °C and (c) 1260 °C.

$(Li_2SnO_3)_{ss}$ also because it owns a typical morphology of the compound Li_2SnO_3 [3,23] and Li_2SnO_3-based solid solutions [9,23]. A slight amount of $(MgO)_{ss}$ in Fig. 4(b), as confirmed by the XRD pattern in Fig. 2(c) and EDS result (Grain D) in Table 2 and Fig. S2(d), cannot be easily detected from its grain morphology because of its limited amount and similar polygonal morphology as L_4MS [7,16,28]. By comparison, rod-like grains become much larger in Fig. 4(c) owing to the grain growth of Li_2SnO_3(ss) with increasing sintering temperature. Different from Fig. 4(b), a few polygonal grains (Grain F) in Fig. 4(c) are only the $(MgO)_{ss}$ phase, rather than L_4MS, as confirmed by EDS results in Fig. S2(f). If Grains B and E are compared, one may find that the content of MgO in $(Li_2SnO_3)_{ss}$ increases with increasing sintering temperature (Table 2). However, the content of Li_2SnO_3 in $(MgO)_{ss}$ changes little with increasing temperature if one carefully looks at Grains D and F. This result keeps consistency with the variation of lattice parameters and cell volume shown in Table 1. Nevertheless, it can be seen that the observation of grain morphology with changing sintering temperature keeps good consistency with the XRD analysis, also further supporting the analysis of the evolution of microwave dielectric properties in Fig. 3.

Although a pure-phase L_4MS powder was synthesized, a single-phase well-densified L_4MS ceramic was not yet obtained because of its high-temperature decomposition. Therefore, the low-temperature sintering technique will be of much interest. Fig. 5 shows the sample density of LMS + x wt.% LiF ceramics varying with changing sintering temperature. The addition of a slight amount of LiF ($1 < x \leq 3$) can effectively reduce the sintering temperature down to ~1000 °C, but more amount of LiF can further decrease the sintering temperature close to ~850 °C, indicating that LiF is an effective sintering aid in Li-based rock salt dielectric ceramics [7,18,28]. Previous studies have demonstrated that LiF sintering aid provides a typical liquid-phase sintering mechanism [7]. The SEM images in Fig. 6 indicate that the $x = 2.0$ and $x = 5.0$ samples have been well densified as sintered at 1000 °C and 850 °C, respectively. The former can be found to have an obviously larger grain size than the latter because of a higher sintering temperature.

Fig. 7 shows the XRD patterns of L_4MS ceramics doped with x wt. % LiF as sintered at different temperatures. For LiF aided L_4MS samples sintered at 1000 °C, a single-phase L_4MS phase can be clearly observed as compared with the pure-phase L_4MS powder and the standard pattern (JCPDS No. 37-1164). For those sintered at 850 °C, a slight amount of impurity phase Li_2SnO_3 (or $(Li_2SnO_3)_{ss}$) appears in addition to the main phase of L_4MS because Li_2SnO_3 tends to preferentially exist at lower temperatures in Li_2O-SnO_2-MgO system. The appearance of the impurity phase should have no much to do with the addition of LiF because there is no chemical reaction between LiF and Li-based rock-salt compounds [7].

Fig. 8 shows the variation of ε_r and Qxf as a function of sintering temperature for L_4MS + x wt.% LiF ceramics. Generally similar to the trend of density with sintering temperature, ε_r and Qxf can reach two optimum values (ε_r = ~13.7, Qxf = ~97,000 GHz; ε_r = ~13.9, Qxf = 146,000 GHz) at 850 °C and 1000 °C for samples with higher LiF content ($x \geq 4$) and lower LiF content ($x \leq 3$), respectively. It seems that ε_r

Table 2
The EDS data of marked grains in L_4MS ceramics sintered at different T_s as indicated in Fig. 4.

T_s (°C)	Spots	Atom (%)				
		Sn	Mg	O	Sn:Mg	Composition
1180	A	16.3(± 0.5)	10.3(± 0.6)	72.3(± 0.7)	1.58	$Li_4MgSn_2O_7$
1215	B	20.4(± 0.5)	1.9(± 0.5)	76.9(± 0.8)	10.7	$(Li_2SnO_3)_{ss}$
	C	19.0(± 0.6)	10.6(± 0.6)	69.3(± 0.7)	1.79	$Li_4MgSn_2O_7$
	D	17.3(± 0.7)	13.2(± 0.6)	68.4(± 0.6)	1.30	$(MgO)_{ss}$
1260	E	19.9(± 0.6)	4.5(± 0.3)	74.3(± 0.7)	4.42	$(Li_2SnO_3)_{ss}$
	F	16.8(± 0.5)	12.3(± 0.4)	69.6(± 0.7)	1.36	$(MgO)_{ss}$

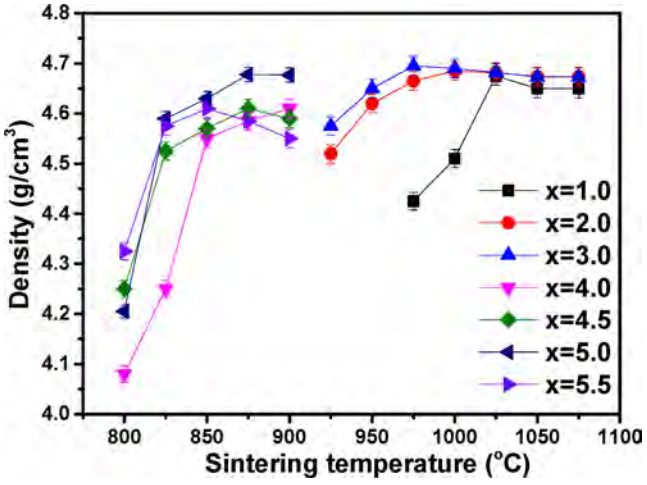

Fig. 5. The bulk density of L_4MS + x wt.% LiF ceramics varying with increasing sintering temperature.

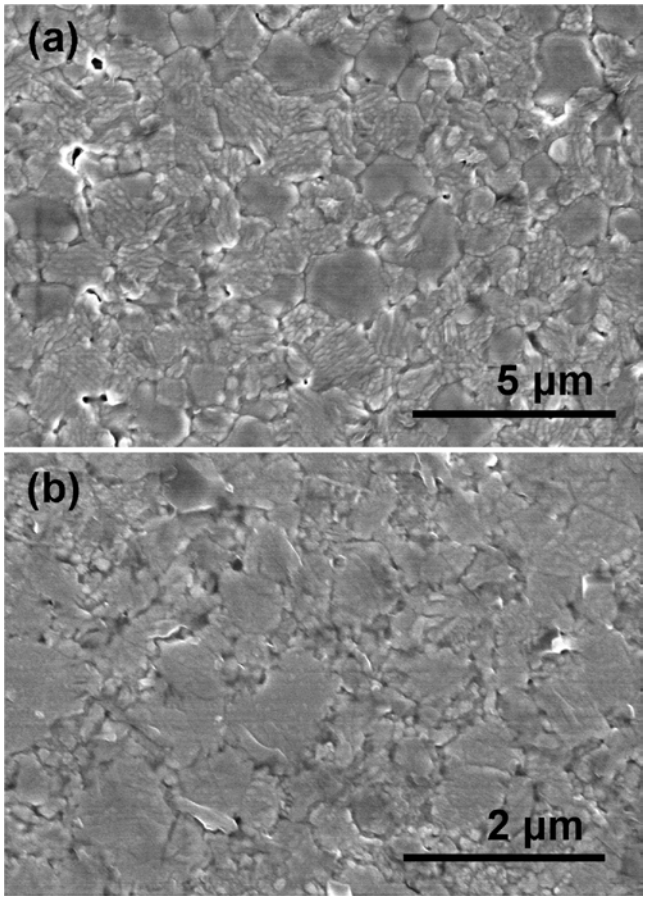

Fig. 6. SEM graphs of L_4MS-x wt.% LiF ceramics sintered at various temperatures: (a) x = 2.0, at 1000 °C and (b) x = 5.0, at 850 °C.

is not as sensitive to the phase composition and grain size as Qxf if one compares these two samples. The big difference between Qxf values of samples densified at higher and lower sintering temperatures might be ascribed to the grain size and the impurity phase, supposed that two samples have similar relative densities. The fine grain size observed in L_4MS samples with x ≥ 4 LiF would increase the extrinsic loss due to the grain boundary fraction. In addition, a higher content of sintering aid LiF might cause the formation of more glass phases in the sample at room temperature after sintering, further reducing their Qxf values.

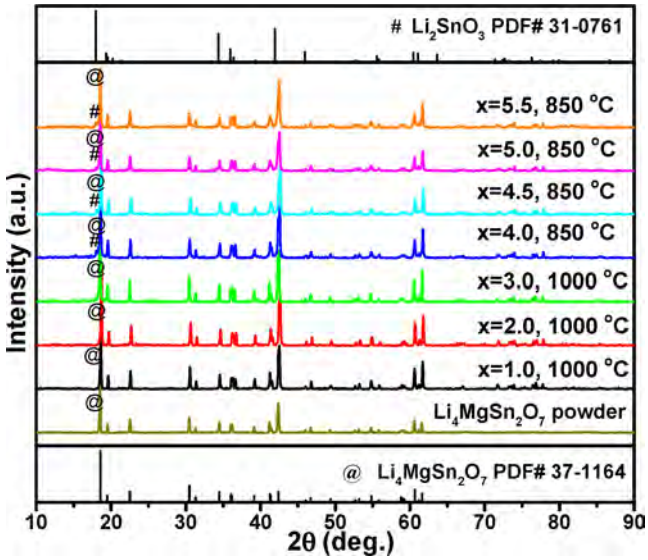

Fig. 7. XRD patterns of L_4MS + x wt.% LiF ceramics sintered at various temperatures as compared with the calcined L_4MS powder and the standard patterns of L_4MS and Li_2SnO_3.

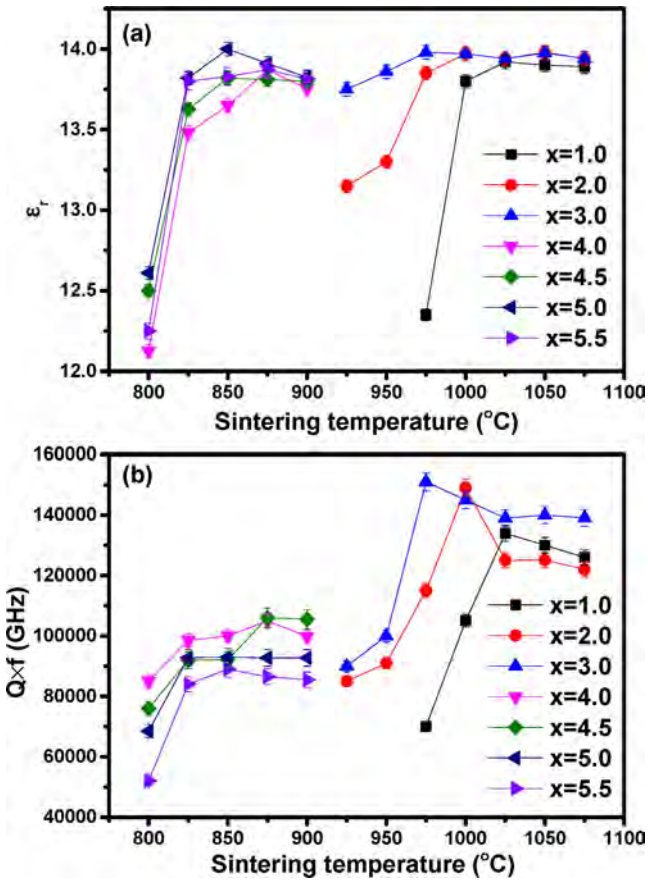

Fig. 8. The variation of (a) ε_r and (b) Q × f values for L_4MS + x wt.% LiF ceramics as a function of sintering temperature.

Moreover, the appearance of a slight amount of $(Li_2SnO_3)_{ss}$ might contribute to a slight reduction of τ_f from 13.4 ppm/°C typical for single-phase L_4MS to 1.2 ppm/°C (x = 5.5) (Fig. 9), although Li_2SnO_3 has a larger positive τ_f but it is greatly reduced in $(Li_2SnO_3)_{ss}$ as a result of decreased structure order degree [4,9,23,29].

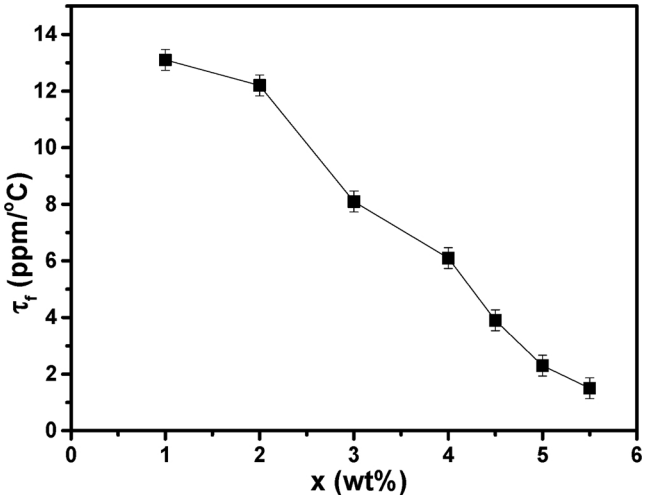

Fig. 9. The τ_f values of L_4MS + x wt.% LiF ceramics sintered at optimum sintering temperatures.

4. Conclusions

In present work, a pure-phase L_4MS was successfully synthesized through optimizing the calcination condition. The phase composition, microstructure and microwave dielectric properties of L_4MS ceramics with sintering temperature have been investigated. An appropriate calcination condition was believed to be 1000 °C for 16 h, ensuring the complete reaction between Li_2SnO_3 and MgO and avoiding the high-temperature decomposition of L_4MS as well. The ceramic sample maintains a single L_4MS phase and thus a constant τ_f of ~12.4 ppm/°C as sintering temperature is below 1200 °C. The appearance of impurity phases, especially $Li_2Mg_3SnO_6$ at higher sintering temperatures tailors τ_f to near zero. The evolution of phase composition was identified by means of Rietveld structure refinement and observation of grain morphology as well as EDS analysis. Excellent microwave dielectric properties of $\varepsilon_r = 13.1 \sim 13.5$, $Q \times f = 106{,}800 \sim 126{,}810$ GHz and $\tau_f = 0 \sim -4.2$ ppm/°C are obtained in samples sintered at 1215 ~ 1260 °C for 4 h. Reduction of sintering temperature using LiF sintering aid helps achieve pure-phase dense L_4MS ceramic. The L_4MS + x wt.% LiF ceramic exhibits $\varepsilon_r \sim 13.7$, Qxf ~ 97,000 GHz ($x \leq 3$) and $\tau_f \sim 8$-13 ppm/°C sintered at 850 °C for potential low-temperature cofired ceramic (LTCC) applications, and $\varepsilon_r \sim 13.9$, Qxf ~ 146,000 GHz and $\tau_f \sim 1.5$–6 ppm/°C ($x \geq 4$) as sintered 1000 °C. The experimental results demonstrate that the L_4MS ceramic would be a potential microwave dielectric candidate material with low permittivity and loss and especially positive τ_f value as a valuable τ_f modifier.

Acknowledgements

Financial supportfrom The Anhui Provincial Natural Science Foundation of China (1508085JGD04) is gratefully acknowledged.

Appendix A. Supplementary data

Supplementary material related to this article can be found, in the online version, at doi:https://doi.org/10.1016/j.jeurceramsoc.2018.08.019.

References

[1] L.L. Yuan, J.J. Bian, Microwave dielectric properties of the lithium containing compounds with rock salt structure, Ferroelectrics 387 (2009) 123–129.
[2] J. Liang, W.Z. Lu, Microwave dielectric properties of Li_2TiO_3 ceramics doped with ZnO–B_2O_3 frit, J. Am. Ceram. Soc. 92 (2009) 952–954.
[3] L.X. Pang, D. Zhou, Microwave dielectric properties of low-firing Li_2MO_3 (M = Ti, Zr, Sn) ceramics with B_2O_3-CuO addition, J. Am. Ceram. Soc. 93 (2010) 3614–3617.
[4] J. Zhang, R.Z. Zuo, Low-temperature fired thermal-stable Li_2TiO_3-NiO microwave dielectric ceramics, J. Mater. Sci.: Mater. Electron. 27 (2016) 7962–7968.
[5] J.J. Bian, Y.F. Dong, Sintering behavior, microstructure and microwave dielectric properties of $Li_{2+x}TiO_3$ ($0 \leq \times \leq 0.2$), Mater. Sci. Eng. B 176 (2011) 147–151.
[6] J. Song, J. Zhang, R.Z. Zuo, Ultrahigh Q values and atmosphere-controlled sintering of $Li_{2(1+x)}Mg_3ZrO_6$ microwave dielectric ceramics, Ceram. Int. 43 (2017) 2246–2251.
[7] R.Z. Zuo, J. Zhang, J. Song, Y.D. Xu, Liquid-phase sintering, microstructural evolution, and microwave dielectric properties of $Li_2Mg_3SnO_6$-LiF ceramics, J. Am. Ceram. Soc. 101 (2018) 569–576.
[8] N.X. Xu, J.H. Zhou, H. Yang, Q.L. Zhang, M.J. Wang, L. Hu, Structural evolution and microwave dielectric properties of MgO–LiF co-doped Li_2TiO_3 ceramics for LTCC applications, Ceram. Int. 40 (2014) 15191–15198.
[9] C.W. Liu, N.X. Wu, Y.L. Mao, J.J. Bian, Phase formation, microstructure and microwave dielectric properties of Li_2SnO_3-MO (M = Mg, Zn,) ceramics, J. Electroceram. 32 (2014) 199–204.
[10] J.X. Bi, C.F. Xing, C.H. Yang, H.T. Wu, Phase composition, microstructure and microwave dielectric properties of rock salt structured Li_2ZrO_3–MgO ceramics, J. Eur. Ceram. Soc. 38 (2018) 3840–3846.
[11] J.J. Bian, Y.F. Dong, New high Q microwave dielectric ceramics with rock salt structures: $(1-x)Li_2TiO_3 + xMgO$ system ($0 \leq \times \leq 0.5$), J. Eur. Ceram. Soc. 30 (2010) 325–330.
[12] C.L. Huang, Y.W. Tseng, J.Y. Chen, High-Q dielectrics using ZnO-modified Li_2TiO_3 ceramics for microwave applications, J. Eur. Ceram. Soc. 32 (2012) 3287–3295.
[13] Z.X. Fang, B. Tang, Y. Yuan, X. Zhang, S.R. Zhang, Structure and microwave dielectric properties of the $Li_{2/3(1-x)}Sn_{1/3(1-x)}Mg_xO$ systems (x = 0–4/7), J. Am. Ceram. Soc. 101 (2018) 252–264.
[14] H.T. Wu, E.S. Kim, Correlations between crystal structure and dielectric properties of high-Q materials in rock-salt structure Li_2O-MgO-BO_2 (B=Ti, Sn, Zr) systems at microwave frequency, RSC Adv. 6 (2016) 47443.
[15] J.J. Bian, L. Wang, L.L. Yuan, Microwave dielectric properties of $Li_{2+x}Ti_{1-4x}Nb_{3x}O_3$ ($0 \leq x \leq 0.1$), Mater. Sci. Eng. B 164 (2009) 96–100.
[16] Z.F. Fu, P. Liu, J.L. Ma, X.G. Zhao, H.W. Zhang, Novel series of ultra-low loss microwave dielectric ceramics: $Li_2Mg_3BO_6$ (B = Ti, Sn, Zr), J. Eur. Ceram. Soc. 36 (2016) 625–629.
[17] Z.F. Fu, P. Liu, J.L. Ma, X.M. Chen, H.W. Zhang, New high Q low-fired $Li_2Mg_3TiO_6$ microwave dielectric ceramics with rock salt structure, Mater. Lett. 164 (2016) 436–439.
[18] Y.X. Mao, H.L. Pan, Y.W. Zhang, Q.Q. Liu, H.T. Wu, Effects of LiF addition on the sintering behavior and microwave dielectric properties of $Li_2Mg_3SnO_6$ ceramics, J. Mater. Sci.: Mater. Electron. 28 (2017) 13278–13282.
[19] J.G. Guo, W.B. Ma, M.J. Ma, H.D. Zhao, Y.X. Yang, J.F. Gao, Sintering characteristic and microwave dielectric properties of ultra-low loss $Li_2Mg_3TiO_6$ ceramic prepared by reaction-sintering process, J. Mater. Sci.: Mater. Electron. 29 (2018) 3640–3647.
[20] S. George, M.T. Sebastian, Synthesis and microwave dielectric properties of novel temperature stable high Q, $Li_2ATi_3O_8$ (A = Mg, Zn) ceramics, J. Am. Ceram. Soc. 93 (2010) 2164–2166.
[21] H.C. Xiang, C.C. Li, C.Z. Yin, Y. Tang, L. Fang, A reduced sintering temperature and improvement in the microwave dielectric properties of $Li_2Mg_3TiO_6$ through Ge substitution, Ceram. Inter. 44 (2018) 5817–5821.
[22] H.F. Zhou, X.H. Tan, J. Huang, X.L. Chen, Sintering behavior, phase evolution and microwave dielectric properties of thermally stable Li_2O-3MgO-mTiO_2 ceramics ($1 \leq m \leq 6$), Ceram. Int. 43 (2017) 3688–3692.
[23] M. Castellanos, A.R. West, Compound and solid solution formation in the system, Li_2SnO_3-MgO, J. Mater. Sci. Lett. 3 (1984) 786–788.
[24] J. Zhang, R.Z. Zuo, J. Song, Y.D. Xu, M. Shi, Low-loss and low-temperature firable $Li_2Mg_3SnO_6$-$Ba_3(VO_4)_2$ microwave dielectric ceramics for LTCC applications, Ceram. Inter. 44 (2018) 2606–2610.
[25] H.T. Kim, Y. Kim, M. Valant, D. Suvorov, Titanium incorporation in Zn_2TiO_4 spinel ceramics, J. Am. Ceram. Soc. 84 (2001) 1081–1086.
[26] H.F. Zhou, X.B. Liu, X.L. Chen, L. Fang, Y.L. Wang, $ZnLi_{2/3}Ti_{4/3}O_4$: a new low loss spinel microwave dielectric ceramic, J. Eur. Ceram. Soc. 32 (2012) 261–265.
[27] A. Kan, T. Moriyama, S. Takahashi, H. Ogawa, Low-temperature sintering and microwave dielectric properties of MgO ceramic with LiF addition, J. Appl. Phys. 50 (2011) 09NF02.
[28] J.X. Bi, C.C. Li, Y.H. Zhang, C.F. Xing, C.H. Yang, H.T. Wu, Crystal structure, infrared spectra and microwave dielectric properties of ultra low-loss $Li_2Mg_4TiO_7$ ceramics, Mater. Lett. 196 (2017) 128–131.
[29] Z.F. Fu, P. Liu, J.L. Ma, B.C. Guo, X.M. Chen, H.W. Zhang, Microwave dielectric properties of low-fired Li_2SnO_3 ceramics co-doped with MgO–LiF, Mater. Res. Bull. 77 (2016) 78–83.